

Contents lists available at ScienceDirect

Materials Science & Engineering A

journal homepage: www.elsevier.com/locate/msea



Nanocrystallization mechanism of beta phase in Ti-6Al-4V subjected to severe plastic deformation



Yingang Liu, Miaoquan Li*

School of Materials Science and Engineering, Northwestern Polytechnical University, Xi'an 710072, PR China

ARTICLE INFO

Article history: Received 15 April 2016 Received in revised form 19 May 2016 Accepted 20 May 2016 Available online 21 May 2016

Keywords:
Titanium alloys
High energy shot peening
Electron microscopy
Grain refinement
Body-centered cubic
Mechanism

ABSTRACT

Nanocrystallization mechanism of beta phase in the bulk coarse-grained Ti-6Al-4V by high energy shot peening was investigated via high-resolution transmission electron microscopy. The results suggested that dislocation gliding was first initiated in beta phase at and around the intersections of the phase boundary with the high-density dislocation structures in alpha phase followed by the formation of dislocation tangles and dislocation walls. As the short axis sizes of alpha phase approached that of beta phase, the dislocation tangles and dislocation walls gradually evolved into the high-angle grain boundaries and subdivided the original grains into the equiaxed ultrafine grains. Under the ultrahigh strain and strain rate, the equiaxed ultrafine grains were eventually refined to randomly oriented nanograins via dynamic recrystallization. In addition, the nanograins would be further refined via dislocation motion upon further straining.

© 2016 Elsevier B.V. All rights reserved.

1. Introduction

Metallic materials with a nanocrystalline structure have high hardness and strength, good tribological properties and good superplasticity at low temperature compared to their coarse grained counterparts [1,2]. Shot peening (SP) as a typical surface mechanical treatment (SMT) method is widely used industrially and is an effective approach to acquire the ultrafine grained or nanostructured surface layer in the bulk metallic materials. SP has been successfully applied to various metallic material systems, such as AISI 4340 [3], AISI 304 steel [4], C-2000 superalloy [5], Ti-4AI-2V [6], TC17 alloy [7] and so on.

Generally speaking, in order to attain a desired nanostructured microstructure, it is absolutely important to understand SPD induced nanocrystallization mechanisms. Comprehensive investigations of nanocrystallization mechanisms in a large number of metallic materials have been demonstrated that dislocation activities, mechanical twinning and phase transformations play the key roles [3,8–11]. Titanium and its alloys have attracted great attention with regard to their excellent performance and comprehensive applications [12,13]. Hence, it is very promising and attractive to produce a nanostructured surface layer in titanium and its alloys for further improving their corrosion resistance, wear resistance and fatigue performance [14,15]. In recent years,

the nanocrystallization mechanisms of titanium and its alloys have been explored by some researchers owing to their considerable scientific and practical interests [8,15–17]. However, the investigations have mainly focused on alpha (α) phase up to now and the preoccupation is barely given for beta (β) phase. Meanwhile, though the nanocrystallization mechanism of β singlephase titanium alloy has been investigated [17], the nanocrystallization mechanism of β phase in dual-phase titanium alloys is still unclear. It is known that α phase and β phase coexist in dual-phase titanium alloys and α phase consequentially influence the deformation of β phase.

The objective of the present work is to exhibit a systematical investigation on the nanocrystallization mechanism of β phase in dual-phase titanium alloys. To perform this aim, high energy shot peening (HESP) and Ti-6Al-4V (the most widely used titanium alloy) are chosen in this study. Transmission electron microscope (TEM) and high-resolution TEM (HRTEM) investigations of the structure characteristics of β phase in Ti-6Al-4V at various depths below the processed surface have been conducted and analyzed in depth.

2. Experimental procedure

The chemical composition (wt%) of as-received Ti-6Al-4V bar with a diameter of 40.0 mm was shown in Table 1. The plate specimens with the dimensions of $70 \text{ mm} \times 19 \text{ mm} \times 4 \text{ mm}$ were

^{*} Corresponding author. E-mail address: honeymli@nwpu.edu.cn (M. Li).

Table 1. The chemical composition of as-received Ti-6Al-4V (wt%).

Al	V	Fe	С	N	0	Н	Ti
6.41	4.19	0.02	0.006	0.001	0.16	0.002	Bal.

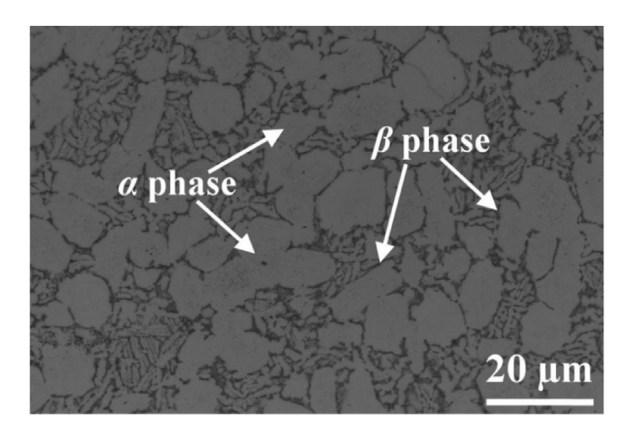


Fig. 1. The as-annealed microstructure of Ti-6Al-4V.

manufactured from the as-received Ti-6Al-4V bar and annealing treated at a heating temperature of 873 K for 1 h following air-cooling to room temperature. The as-annealed microstructure of Ti-6Al-4V specimens shown in Fig. 1 consisted of predominantly high volume fraction of hexagonal close-packed (hcp) α phase with an average grain size of 9.37 μ m and a small amount of body-centered cubic (bcc) β phase with a total volume fraction of about 14.3% distributing in α grain boundaries.

Then, the Ti-6Al-4V specimens were processed via HESP in a MP6000PT air blast machine. During HESP, the standard cast steel shots ASH230 with a diameter of 0.6 mm were violently accelerated at an air pressure of 0.25 MPa and a processing duration of 60 min, and the peening nozzle with a diameter of 10 mm and the mass flow rate of 10 kg/min were adopted.

The cross-section TEM foil with the dimension of 19 mm \times 4 mm \times 0.5 mm perpendicularly to the processed surface was cut from the Ti-6Al-4V HESP processed specimen, and polished an overall thickness of 30 μm at first, followed by bonding with a copper loop with a diameter of 3 mm, and finally the foil was perforated at the processed surface layer via ion thinning with proper incident angles. TEM and HRTEM observations of the HESP processed Ti-6Al-4V were carried out on a Tecnai F30 G2 field emission transmission electron microscope operated at an acceleration voltage of 300 kV.

3. Results and discussion

3.1. 110 μ m and more below the processed surface

Fig. 2(a) and (b) shows the bright-field (BF) image of microstructure characteristics which are adjacent to the strain-free matrix at a depth of about 150 μ m below the processed surface. As seen from Fig. 2(a) and (b), the elongated β grains are extremely small and with the grain size mainly ranging from 200 nm to 400 nm. Meanwhile, none of crystal defects are observed inside β grains. However, for α phase with an average grain size of 9.37 μ m, the dislocations have been observed. As a result, it is clear that the plastic deformation first occurs in α phase during HESP. This phenomenon is attributed to the fact that the grain size of β phase is far smaller than that of α phase though β phase is soft phase with more easily activated independent slip systems, i.e., the

deformation resistance for β phase is larger than that for α phase under the low strain and strain rate. Therefore, it implies that the grain size plays a key role in determining the deformation behavior of Ti-6Al-4V under the low strain and strain rate. Furthermore, as seen from Fig. 2(a), the dislocations in α phase mainly exist near the phase boundary (PB) between α phase and β phase as indicated by the black arrowheads and the dash dotted line marks PB. It suggests that the dislocations in α phase mainly nucleate and pile up at the PB, where the local stress concentration is developed.

With the decreasing of depth below the processed surface accompanied by an increase in the strain and strain rate, high-density dislocations occur in α phase and impact on PBs. As the local stress concentration exceeds the critical shear strength of β phase, slip systems are activated inside β phase and two typical dislocation structures are observed as shown in Fig. 2(c) and (d). The first one is dislocation tangles (DTs) that the dislocations are intertwined in a completely complex way as seen from Fig. 2(c) and DTs are frequently observed in β phase. The second one is dislocation wall (DW) that the dislocations have the same slip planes and directions as seen from Fig. 2(d). It is noticed that DTs and DW are the main dislocation structures in the materials with bcc structure such as Fe [18], 40Cr alloy [19] and NiTi alloy [20]. Meanwhile, it should be also underlined that the dislocation gliding in β phase generally initiates at and around the intersections of the PB with the high-density dislocation structures such as DTs in α phase by extensive TEM observations. This is consistent with the fact that high stress concentrations developed at the PB due to the intersection with the DTs in α phase make the dislocations in β phase nucleate easily. In addition, comparing with β single-phase titanium alloy [17], twinning has not participated in the deformation of β phase in Ti-6Al-4V during HESP. Apparently, as for bcc β phase with high stacking fault energy and more slip systems, dislocation gliding is the main deformation mechanism. It is widely accepted that the twinning will coordinate deformation as the dislocation gliding cannot maintain the homogeneous plastic deformation [21,22]. The non-coherent PB due to the large difference of crystal structure offers massive nucleation sites of dislocations for β phase in Ti-6Al-4V. Therefore, it is reasonable to confirm that the dislocation gliding can coordinate the deformation of β phase in Ti-6Al-4V during HESP, resulting in the absence of twinning.

At a depth of about 110 μm below the processed surface, because the dislocation activities are more severe in α phase and lots of DTs and subgrain boundaries (SGBs) occur in α phase, more and more high-density dislocation structures are generated and trapped in β phase as indicated by the black arrowheads and shown in Fig. 2(d). Such a coincidence further supports that the occurrence of dislocation gliding in β phase is owing to the intersections of PB with the DTs in α phase. Meanwhile, it is also worth noting that the high-density dislocation structures in β phase have divided the original grains into equiaxed domains as seen from Fig. 2(d). In addition, the selected area electron diffraction (SAED) patterns demonstrated in the insets of Fig. 2(c)-(e) indicate that the DTs and DW have not transformed into the SGBs at a depth of about 110 μ m below the processed surface.

3.2. 80 µm below the processed surface

As the strain and strain rate increase with the decreasing of depth below the processed surface, the microstructure mainly consists of the elongated and approximately parallel ultrafine grains (UFGs) as shown in Fig. 3. Meanwhile, with progressive refinement of α phase at a depth of about 80 μ m below the processed surface, the short axis sizes of α phase approach that of β phase. The misorientation angles of 5.6° and 6.8° reveal the

Download English Version:

https://daneshyari.com/en/article/1573344

Download Persian Version:

https://daneshyari.com/article/1573344

<u>Daneshyari.com</u>